



Deformation and spallation of a magnesium alloy under high strain rate loading

M. Wang^{a,b,c}, L. Lu^{c,e}, C. Li^{a,c}, X.H. Xiao^d, X.M. Zhou^c, J. Zhu^{a,*}, S.N. Luo^{b,c,**}

^a College of Physical Science and Technology, Sichuan University, Chengdu, Sichuan 610064, PR China

^b Key Laboratory of Advanced Technologies of Materials, Ministry of Education, Southwest Jiaotong University, Chengdu, Sichuan 610031, PR China

^c The Peac Institute of Multiscale Sciences, Chengdu, Sichuan 610031, PR China

^d Advanced Photon Source, Argonne National Laboratory, Argonne, IL 60439, USA

^e CAS Key Laboratory of Mechanical Behavior and Design of Materials, Department of Modern Mechanics, University of Science and Technology of China, Hefei, Anhui 230027, PR China

ARTICLE INFO

Article history:

Received 1 November 2015

Received in revised form

24 January 2016

Accepted 2 March 2016

Available online 3 March 2016

Keywords:

Magnesium alloys

Twinning

Strain rate

Impact

EBSD

ABSTRACT

We investigate deformation and damage of a magnesium alloy, AZ91, under high strain rate ($\sim 10^5 \text{ s}^{-1}$) loading via planar impact. The soft-recovered specimens are examined with electron back-scatter diffraction (EBSD). EBSD analysis reveals three types of twinning: $\{10\bar{1}2\}$ extension, $\{10\bar{1}1\}$ contraction, and $\{10\bar{1}1\}$ – $\{10\bar{1}2\}$ double twinning, and their number density increases with increasing impact velocity. The extension twins dominate contraction and double twins in size and number. Dislocation densities of the recovered specimens are evaluated with x-ray diffraction, and increase with increasing impact velocity. X-ray tomography is used to resolve three-dimensional microstructure of shock-recovered samples. The EBSD and tomography results demonstrate that the second phase, $\text{Mg}_{17}\text{Al}_{12}$, plays an important role in both deformation twinning and tensile cracking. Deformation twinning appears to be a common mechanism in deformation of magnesium alloys at low, medium and high strain rates, in addition to dislocation motion.

© 2016 Elsevier B.V. All rights reserved.

1. Introduction

Magnesium alloys show a remarkable potential for their low density, high specific strength, and high specific stiffness [1,2]. Normally used as die cast products (e.g., AZ91), they offer a combination of desirable mechanical properties, castability and corrosion resistance [3,4]. During service, magnesium alloys may be subjected to impulsive loading such as impact, and their dynamic responses under high strain rate loading have been investigated with split Hopkinson compression or tension bars (10^2 – 10^4 s^{-1}) [5–9], and to a lesser extent, with gas gun plate impact at higher strain rates ($\sim 10^5 \text{ s}^{-1}$ or higher) [10–15].

Under one-dimensional (1D) strain shock loading, dynamic tensile strength or spall strength of Mg95 (99.95 wt.% Mg) was studied over a wide range of temperatures [10]. The shear strength of magnesium alloy AZ61 was observed to increase with increasing peak shock stress [12]. The effects of orientation and heat treatment on the Hugoniot elastic limit and spall strength of

* Corresponding author.

** Corresponding author at: The Peac Institute of Multiscale Sciences, Chengdu, Sichuan 610031, PR China.

E-mail addresses: zhujun01@163.com (J. Zhu), sluo@pims.ac.cn, sluo@swjtu.cn (S.N. Luo).

magnesium alloy Elektron 675 were examined, and their values are higher along the extrusion direction [13]. The elastic precursor decay in magnesium alloy Ma2-1 under shock compression was explored for different sample thicknesses [14]. Such planar impact studies provide useful information on bulk mechanical properties of magnesium alloys. However, shock-induced microstructure changes and deformation mechanisms are rarely addressed, despite their apparent importance for high strain rate applications.

In cast magnesium alloy AZ91, the main strengthening intermetallic (the second phase) is β - $\text{Mg}_{17}\text{Al}_{12}$ dispersed within grains or at grain boundaries. This body-centered cubic structure of $\text{Mg}_{17}\text{Al}_{12}$ is incompatible with the close-packed hexagonal (HCP) structure of the magnesium matrix. In Hopkinson bar tests, the $\text{Mg}/\text{Mg}_{17}\text{Al}_{12}$ interface acts as the crack initiation site in AZ91 alloy [7]; increasing the volume fraction of β - $\text{Mg}_{17}\text{Al}_{12}$ leads to an increase in yield strength and strain hardening, but a decrease in ductility and the twin fraction in AZ magnesium alloys under compression [16].

Deformation twinning modes in magnesium include $\{10\bar{1}2\}$ extension twinning, $\{10\bar{1}1\}$ contraction twinning [17,18], and $\{10\bar{1}1\}$ – $\{10\bar{1}2\}$ double twinning [6,7,19–25], in the order of increasing difficulty in activation. It is the easiest to activate $\{10\bar{1}2\}$ extension twinning at various strain rates, and $\{10\bar{1}1\}$ contraction twinning is observed in *c*-axis compression of pure magnesium

single crystals and polycrystalline magnesium alloys [17,26,27]. Contraction twinning and double twinning are often observed in uniaxial tension, while extension twinning prevails in uniaxial compression and ring hoop tension testing [20]. $\{10\bar{1}1\}$ – $\{10\bar{1}2\}$ double twinning is responsible for shear failure of magnesium alloy AZ31 at room temperature, and yet $\{10\bar{1}2\}$ extension twinning has little influence on void formation [22]. Hopkinson bar tests revealed that increasing strain rate ($\sim 10^3 \text{ s}^{-1}$) enhances the activation of $\{10\bar{1}2\}$ extension twinning dramatically, while its effects on contraction and double twinning are insignificant [6].

At high strain rates comparable to gas gun loading (10^4 – 10^7 s^{-1}), few experiments have investigated deformation mechanisms of magnesium alloys in general. In this work, we explore high strain rate deformation of magnesium alloy AZ91 with gas-gun plate impact loading at different impact velocities (170–265 ms^{-1}). The shock-recovered samples are examined with electron backscatter diffraction (EBSD), x-ray tomography and diffraction. While $\{10\bar{1}2\}$ extension twinning still dominates deformation, $\{10\bar{1}1\}$ contraction twinning and $\{10\bar{1}1\}$ – $\{10\bar{1}2\}$ double twinning also occur at higher impact velocities. The number density of twins and dislocation density increase with increasing impact velocity. The second phase, $\text{Mg}_{17}\text{Al}_{12}$, plays an important role in both deformation twinning and tensile cracking.

2. Materials and experiments

The cast magnesium alloy AZ91 in this work contains 9.0 wt% Al, 0.6 wt% Zn, 0.4 wt% Mn, and 90.0 wt% Mg. The initial microstructure is analyzed with EBSD (Fig. 1(a)). Its grain size ranges from 100 μm to 500 μm with abundant β - $\text{Mg}_{17}\text{Al}_{12}$ phase

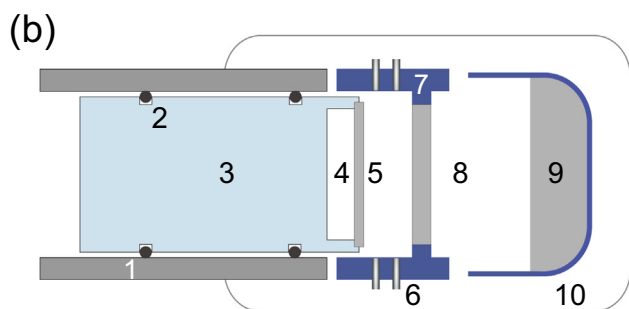
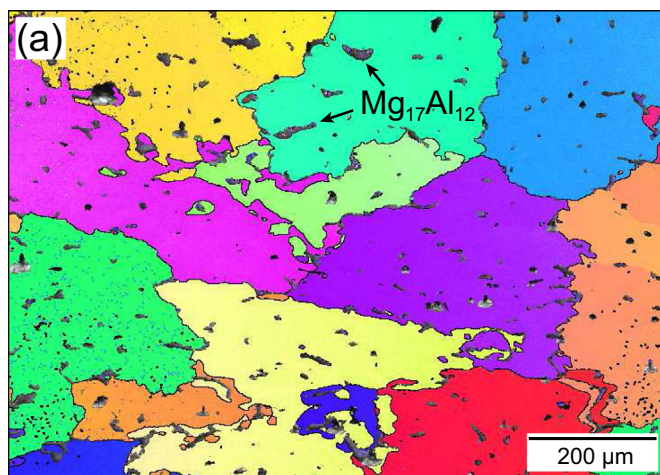


Fig. 1. (a) EBSD orientation map of an as-received AZ91 specimen. (b) Schematic setup of gas-gun plate-impact experiments. 1: gun barrel; 2: O-ring; 3: polycarbonate sabot; 4: recess for release waves; 5: flyer plate; 6: optical fibers and detectors for the optical beam block system; 7: sample holder; 8: sample; 9: soft materials; 10: vacuum chamber.

distributed “randomly” in grain interiors or at grain boundaries. Both flyer plates and samples have a diameter of 10 mm and are made of the same batch of AZ91 for symmetric impact. The thicknesses of flyer plates and samples are 0.7 mm and 1.4 mm, respectively. Two parallel surfaces of a target or flyer plate are polished to micron level or mirror finish.

Flyer plate planar impact experiments are conducted with a 10-mm bore, single-stage gas gun to investigate dynamic tension response of the AZ91 samples initially at room temperature. Fig. 1 (b) shows the schematic setup of flyer plate impact experiments. A flyer plate (5) is attached to polycarbonate sabot (3), with a recess (4) immediately behind it. When a solenoid valve is fired, compressed nitrogen is released from a high-pressure gas reservoir into the gun barrel (1), accelerating the sabot and flyer plate assembly. Upon exiting the muzzle, the flyer plate impacts the target or sample (8) under consideration. The flyer plate velocity is measured with an optical beam block system (6). The muzzle and sample are located in a vacuum chamber (10). The shocked samples are “soft” recovered with foams (9) for EBSD, and x-ray tomography and diffraction.

3. Results and discussion

Spallation experiments are conducted at three different impact velocities, 171 ms^{-1} , 218 ms^{-1} and 265 ms^{-1} . When the release fans initiated from the back of the flyer plate and the sample free surface encounter and interact in the midsection of the target, this region undergoes a transition from compression to tension. Once the tensile stress exceeds a critical stress, termed as the spall strength, spall occurs. The methodology as well as data analysis related to planar impact experiments can be found in previous studies [28–31].

During shock loading, there is a shock heating effect. However, the impact velocities are low (the maximum is 265 ms^{-1}) and shock durations are short ($\sim 300 \text{ ns}$). While dynamic recovery of microstructure due to shock heating does exist, it is expected to be small in our experimental conditions. In order to investigate shock-induced microstructure changes of the AZ91 magnesium alloy, the shock-recovered targets are sectioned into halves along the impact direction, and EBSD is utilized to analyze the cross-sections. EBSD inverse pole figures and the corresponding image quality maps of the samples deformed at various impact velocities are shown in Fig. 2. In addition, cracks are observed at grain boundaries and grain boundary triple junctions in the sample impacted at 265 ms^{-1} (Fig. 2(f)), while no obvious cracks are found for lower impact velocities. The second phase tends to conglomerate around grain boundaries, and both are weak spots for tensile microcrack nucleation. Consistently, cracks were found to be prone to nucleate at the Mg/ $\text{Mg}_{17}\text{Al}_{12}$ interfaces [16]. The growth and coalescence of microcracks lead to intergranular cracking.

X-ray tomography is used to investigate microstructure of the spallation region in the shock-recovered specimens. X-ray tomography is a nondestructive 3D technique capable of resolving internal structure with micron resolutions, and conducted at the 2-BM beamline of the Advanced Photon Source. The 3D microstructure reconstructed with tomography is shown in Fig. 3 for the specimen impacted at 265 ms^{-1} , showing three structural components: the magnesium matrix, the second phase ($\text{Mg}_{17}\text{Al}_{12}$), and cracks. The second phase is distributed inhomogeneously, consistent with the EBSD result. Numerous cracks are induced during tension and most of them are surrounded by the second phase, indicating that the interfaces between the second phase and the matrix are the nucleation sites for cracks.

All the regions indicated in Fig. 2 are located in the mid-sections of the targets, which are subjected to tension and possible spall. Under high strain rate tension, the most pronounced

Download English Version:

<https://daneshyari.com/en/article/1573510>

Download Persian Version:

<https://daneshyari.com/article/1573510>

[Daneshyari.com](https://daneshyari.com)